Analysis and Design of Repetitive Controllers for Applications in Distorted Distribution Grids

Philipp Schülting, Christoph H. van der Broeck, and Rik W. De Doncker

***Abstract*—This paper proposes a generalized design procedure for repetitive current controllers in distorted distribution grids to obtain good disturbance rejection properties and well behaved and robust system dynamics. Different implementation options for repetitive controllers (RCs) are discussed based on an accurate discrete time model. A simple control design is derived, which allows any desirable dynamics to be adjusted by one single parameter. Even a deadbeat design is possible. The impact of model inaccuracies and numerical errors on the dynamic and stability of the system is investigated. It is shown that the RC leads to low damping or even instability at high switching frequencies caused by modeling errors or numerical inaccuracies. Based on the stability analysis, it is discussed how to handle these design challenges, which exist especially for RCs of high order. The proposed control structure and control design concept is verified by simulations and experiments.**

***Index Terms*—Current harmonics, modeling, repetitive control.**

I. Introduction

IN RECENT years, the role of pulsewidth modulation (PWM) converters connected to the utility grid (see Fig. 1) has changed fundamentally. The growing number of wind turbines and photovoltaic systems have resulted in more and more converter systems in the distribution grid, which are responsible for the energy conversion of the generated wind and solar power. To prevent a strong distortion of the grid voltage, the regulation IEC 61000-3-4 enforces a limit on the harmonics of the current fed into the grid. According to this regulation, a total harmonic distortion (THD) of 5% must not be exceeded [1]. Among other effects, grid voltage harmonics can excite harmonics in the inverter current. These current harmonics vice versa can further excite voltage harmonics, resulting in a growing grid distortion as more converter systems are connected to the grid. This effect is particularly strong in regions where the grid voltage is not very stiff. Thus, the controller of the PWM converter needs to reject voltage harmonics to prevent the excitation of higher order current harmonics. There are different control topologies to handle this task, e.g., resonant controllers [2] or repetitive controllers (RCs) [3]–[5]. The design approach for these control schemes is more challenging than the design of a conventional synchronous frame PI controller (SFPI). However, in [2], a systematic approach for the control design of resonant controllers based on the root locus method generalized for space vectors has been presented. Although the control design of this resonant controller is straightforward, it requires a certain expertise of the design engineer. In contrast, the RC is able to reject harmonics at multiples of the grid frequency, and requires much less design expertise if a systematic design procedure is used as it is shown in this paper. There are many publications discussing theoretical design concepts for this control topology, e.g., [5]–[10]. However, most approaches deal with the control design aspects on a system-theoretical level and do not give particular insight in the way a RC is implemented based on an accurate discrete time model. Thereby, the presented control design approaches seem rather complex. This paper illustrates a generalized way to optimize the RC for fast disturbance response and high command tracking dynamics. Furthermore, it demonstrates the limits of this control concept, which takes into account implementation aspects, e.g., the impact of modeling errors and numeric precision.

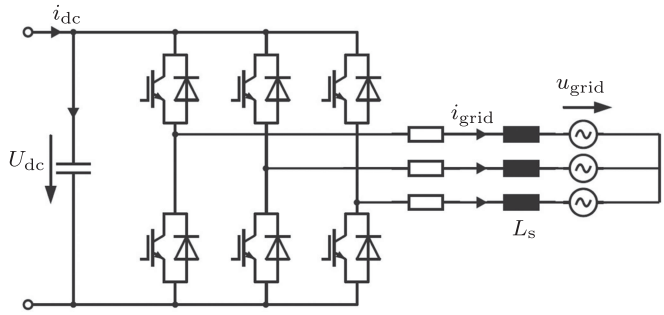

Fig. 1. Three-phase converter with an *L*-filter connected to the utility grid.

For the control design, first, a discrete-time model of the whole system needs to be derived. Then, a PI controller in the synchronous frame will be designed based on the root locus method generalized for space vectors to handle the control of the current at the fundamental frequency. The SFPI controller is optimized to achieve a fast disturbance response and well-behaved dynamics.

After these basic design steps, the RC, which rejects higher order harmonics based on the inner model principle [11]–[13],

Manuscript received August 11, 2017; revised October 6, 2017, December 21, 2017, and February 16, 2018; accepted April 24, 2018. Date of publication May 3, 2018; date of current version November 19, 2018. This paper was presented at COMPEL 2015, Vancouver BC, Canada, titled: "A Generalized Control Design Approach for a Repetitive Controller on Current Harmonics." Recommended for publication by Associate Editor Prof. Y. W. Li. *(Corresponding author: Philipp Schuelting.)*

The authors are with the Institute for Power Electronics and Electrical Drives, RWTH Aachen University, 52066 Aachen, Germany (e-mail:

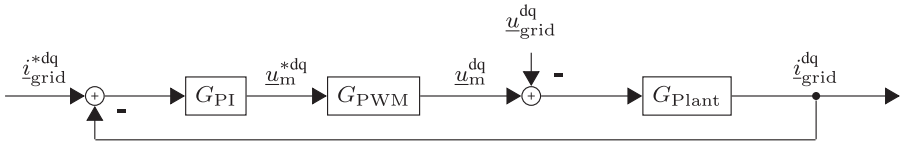

Fig. 2. State block diagram of the converter controlled with a PI controller in the synchronous frame.

is described in the synchronous frame in detail and a filter function will be derived based on the accurate system model to achieve a fast transient behavior. It will be shown that the selected filter function provides a response, which can be tuned up to deadbeat dynamics. The concrete design decision of the resulting RC is made by selecting a simple gain. It is discussed and illustrated how the decision affects the dynamics of the system. Simulations and experiments verify the illustrated theory. A comparison between the system with and without the RC is presented to demonstrate the validity of the proposed concepts.

Finally, it will be demonstrated how modeling errors and numerical aspects influence the performance of the RC and must be taken into account for the control design.

II. Modeling and Control in the Synchronous Frame

First, a general current control system (see Fig. 2) consisting of an SFPI controller, a PWM, and an inductance L_s that represents the plant is investigated. An *L*-filter is used to demonstrate the concept of the proposed design of a RC. Typically, an *LCL*-filter is used as a grid filter but, for most applications, the *LCL*-filter resonance does not have an impact on the control loop because its resonance frequency is located above the control bandwidth. Thus, the filter capacitance is typically neglected for the control design and analysis. For this reason, a converter with an *L*-filter is discussed to keep the mathematical description simple. The transfer functions of this system are derived. $\underline{i}_{\mathrm{grid}}^{*dq}$ is the reference current in the *dq*-frame, $\underline{u}_{\mathrm{m}}^{*dq}$ is the manipulated input voltage by the SFPI controller, $\underline{u}_{\mathrm{m}}^{dq}$ is the delayed manipulated input voltage, $\underline{i}_{\mathrm{grid}}^{dq}$ is the grid current, and $\underline{u}_{\mathrm{grid}}^{dq}$ is the grid voltage modeled as a disturbance for the plant. All variables are defined as space vectors with a real and a complex argument.

The time between sampling of the measured quantities and updating the manipulated input voltage $\underline{u}_{\mathrm{m}}^{\alpha\beta}$ in the s-domain for the stationary reference frame is characterized by a delay [2]

$$\underline{G}_{\mathrm{PWM}}^{\alpha\beta}(s) := \frac{\underline{U}_{\mathrm{m}}^{\alpha\beta}(s)}{\underline{U}_{\mathrm{m}}^{\alpha\beta *}(s)} = \mathrm{e}^{-sT_{\mathrm{s}}} \tag{1}$$

with the sampling rate T_{s}. For the model of the *L*-filter, we assume that the filter has negligible ohmic losses or parasitic elements. This leads to the following complex space vector transfer function of the plant in the s-domain where the modulator is included

$$\underline{G}_{\mathrm{Plant}}^{\alpha\beta}(s) := \frac{\underline{I}_{\mathrm{grid}}^{\alpha\beta}(s)}{\underline{U}_{\mathrm{m}}^{*\alpha\beta}(s)} = \frac{1}{sL_{\mathrm{s}}} \cdot \mathrm{e}^{-sT_{\mathrm{s}}}. \tag{2}$$

The resulting model of the system describes the system dynamics in the stationary frame accurately. Because of the regular sampled PWM, the controlled voltage is held constant over one time step. This latch leads to the discrete-time open loop transfer function

$$\underline{G}_{\mathrm{Plant}}^{\alpha\beta}(z) = \left(1 - z^{-1}\right) \mathscr{Z}\left(\frac{\underline{G}_{\mathrm{Plant}}^{\alpha\beta}(s)}{s}\right) \tag{3}$$

$$\underline{G}_{\mathrm{Plant}}^{\alpha\beta}(z) = \frac{T_{\mathrm{s}}}{L_{\mathrm{s}}} \cdot \frac{z^{-1}}{1 - z^{-1}} \cdot z^{-1}. \tag{4}$$

In [2], it has been shown how a discrete time model formulated in the stationary frame can be transferred from the stationary frame to the synchronous frame. This is practically done by replacing all delays in the stationary frame model by delays with a rotation in the complex plane where $\omega_0 = 2\pi f_0$ is the grid frequency

$$z^{-1}\big|^{\alpha\beta} = z^{-1}\ \mathrm{e}^{-\mathrm{j}\omega_0 T_{\mathrm{s}}}\big|^{\mathrm{dq}}. \tag{5}$$

With this transformation for single delays, the discrete-time transfer function of the plant in the synchronous frame can be written as

$$\underline{G}_{\mathrm{Plant}}^{\mathrm{dq}}(z) = \frac{T_{\mathrm{s}}}{L_{\mathrm{s}}} \cdot \frac{z^{-2}\mathrm{e}^{-\mathrm{j}2\omega_0 T_{\mathrm{s}}}}{1 - z^{-1}\mathrm{e}^{-\mathrm{j}\omega_0 T_{\mathrm{s}}}}. \tag{6}$$

Note that this is a transfer function of space vector quantities which may have complex coefficients. Based on model (6), an SFPI controller can be designed. Therefore, typical design methodologies, e.g., the symmetrical optimum or the root locus method can be used.

As an example, the design procedure for an SFPI controller with the root locus method is shown. For a more detailed discussion of this design procedure, please refer to [2]. The discrete-time SFPI controller can be written as

$$G_{\mathrm{PI}}(z) = K_{\mathrm{p}}\left(1 + \frac{K_{\mathrm{i}}T_{\mathrm{s}}}{K_{\mathrm{p}}} \frac{1}{1 - z^{-1}}\right). \tag{7}$$

Then, the characteristic equation

$$1 + G_0(z) = 1 + G_{\mathrm{PI}}(z)\, G_{\mathrm{PWM}}(z)\, G_{\mathrm{Plant}}(z) = 0 \tag{8}$$

is calculated to obtain the eigenvalues of the system that represents the system dynamic of the controlled system. The ratio $\tau = \frac{K_{\mathrm{i}}T_{\mathrm{s}}}{K_{\mathrm{p}}}$ can be varied as it is shown in Fig. 3. With a fixed value of τ, an increasing proportional gain K_{p} leads to traces of the eigenvalues in the complex plane, the so-called root loci. In Fig. 3, the root loci are shown for different regulation time constants τ. The value K_{p} for a damping of $\xi = 0.707$ is marked. With the root locus method, it can be seen that $K_{\mathrm{P}} = \frac{L_{\mathrm{s}}}{3T_{\mathrm{s}}}$ and

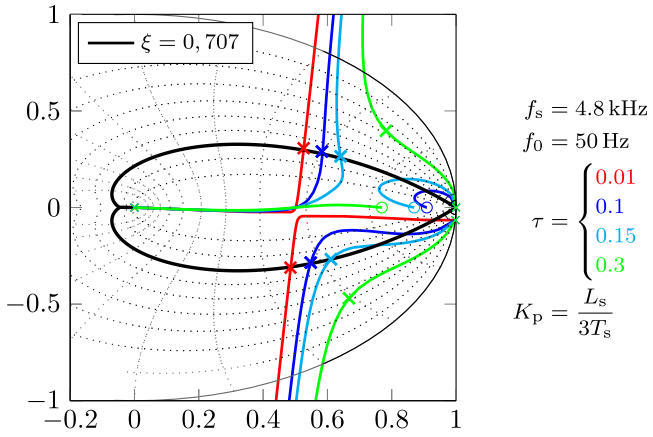

Fig. 3. Root locus design procedure for the SFPI regulator.

$\frac{K_I T_s}{K_P} = 0.15$ results into optimized disturbance rejection properties together with accurate damping. A detailed analysis and discussion of this design method is given in [2]. Hence, these settings will be used for all further considerations.

III. Design of the RC

A. Analytical Description

The RC will be placed in parallel to the SFPI controller as it is shown in Fig. 4. The advantage of the parallel structure is that the output voltage of the proportional path, the integral path, and the resonant paths sum up to the PWM voltage command. So the feedback voltages can be analyzed separately. In many other publications [4], [14], [15], the RC is connected in series to the control error, which does not provide insight into the behavior of all feedback paths. However, both schemes can be used equivalently and achieve identical results.

If the grid voltage exhibits higher order harmonics, the disturbance will cause a periodic grid current error if only an SFPI controller is used. The RC basically consists of a periodic memory, implemented with N delay elements with positive feedback. This structure remembers periodic errors and will compensate for them if they occur again. If the error is not truly compensated after one period, the positive feedback path will ensure a correction such that after another period the compensation will do better. To ensure that the RC is capable of capturing periodic disturbances, it needs to remember one full grid period of $T_0 = 20$ ms for a grid frequency of $f_0 = 50$ Hz. This leads to N storage elements with

$$N = \frac{f_s}{f_0} \tag{9}$$

where f_s is the sampling frequency.

With k_r as a proportional gain to amplify the current error, the transfer function of the RC can be derived as

$$G_{RC}(z) = k_r \frac{z^{-N}}{1 - z^{-N}}. \tag{10}$$

A simple concept to take advantage of the knowledge of periodic errors is to use the inverse of the plants' transfer function (6) to calculate the voltage that is required to compensate the periodic disturbance. This inverse is depicted as the filter function $G_{RC,filter}(z)$ in Fig. 4. Unfortunately, this concept leads to low damped or even unstable eigenvalues. To increase the stability of the system, the filter function needs to be designed taking into account the dynamics of the plant controlled by the SFPI regulator, which was not taken into account in the first approach.

Therefore, the dynamics of the controlled system with the RC shall be reviewed. It is assumed that the transfer function of the RC is given by

$$G_{RC+filter}(z) = k_r \frac{z^{-N}}{1 - z^{-N}} \cdot G_{RC,filter}(z). \tag{11}$$

The eigenvalues of the closed-loop system are given by the characteristic equation

$$1 + G_0(z) = 0 \tag{12}$$

with the open loop transfer function

$$G_0(z) = (G_{PI}(z) + G_{RC+filter}(z)) \cdot G_{PWM}(z) G_{Plant}(z). \tag{13}$$

Using (11)–(13), the following characteristic equation can be derived, which describes the eigenvalues of the closed-loop system:

$$k_r \frac{z^{-N}}{1 - z^{-N}} G_{RC,filter}(z) = -\frac{1 + G_{PI}(z) G_{PWM}(z) G_{Plant}(z)}{G_{PWM}(z) G_{Plant}(z)}. \tag{14}$$

By selecting the filter function of the RC to

$$G_{RC,filter}(z) = \frac{1 + G_{PI}(z) G_{PWM}(z) G_{Plant}(z)}{G_{PWM}(z) G_{Plant}(z)} \tag{15}$$

further mathematical calculation leads to the characteristic equation as follows:

$$\begin{aligned} & k_r \frac{z^{-N}}{1 - z^{-N}} G_{RC,filter}(z) = -\frac{1 + G_{PI}(z) G_{PWM}(z) G_{Plant}(z)}{G_{PWM}(z) G_{Plant}(z)} \\ \Leftrightarrow\ & k_r \frac{z^{-N}}{1 - z^{-N}} \cdot \frac{1 + G_{PI}(z) G_{PWM}(z) G_{Plant}(z)}{G_{PWM}(z) G_{Plant}(z)} \\ & \quad = -\frac{1 + G_{PI}(z) G_{PWM}(z) G_{Plant}(z)}{G_{PWM}(z) G_{Plant}(z)} \\ \Leftrightarrow\ & k_r \frac{z^{-N}}{1 - z^{-N}} = -1 \end{aligned} \tag{16}$$

which finally leads to a simple equation for the pole placement

$$z^N = 1 - k_r. \tag{17}$$

Even this filter function $G_{RC,filter}(z)$ is a complex filter function, the calculation of rearranging of the coefficients can be performed in software. The resulting filter function can be described as

$$G_{RC,filter}(z) = \frac{b_0 z^{-n} + b_1 z^{-n+1} + \cdots + b_{n-1} z^{-1}}{a_0 z^{-n} + a_1 z^{-n+1} + \cdots + a_n} \tag{18}$$

which can easily be implemented in software.

With this particular choice for the filter function $G_{RC,filter}(z)$, the characteristic equation can be separated from the system parameters. Thus, by selecting a proper $k_r \in [0, 2)$, the eigenvalues

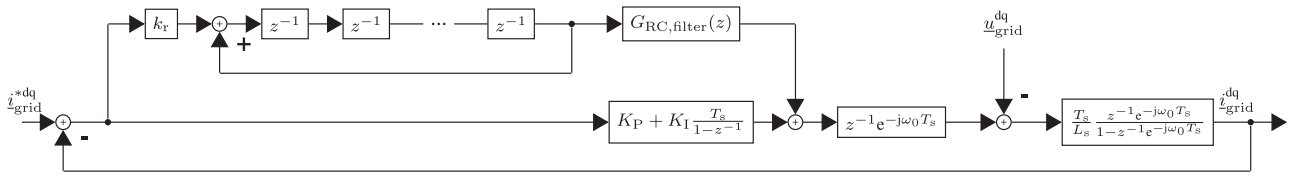

Fig. 4. State block diagram of the studied current control structure.

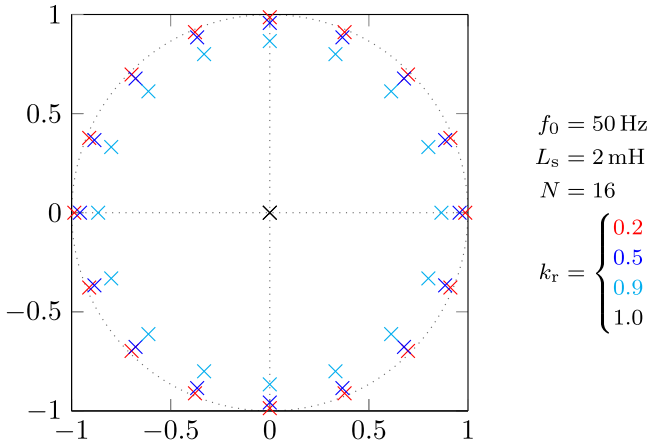

Fig. 5. Eigenvalue migration with variation of k_r.

of the system can be placed to any desirable system performance. The absolute value of the poles is given as

$$|z| = \left| \sqrt[N]{1 - k_\mathrm{r}} \right| \tag{19}$$

which is depicted in Fig. 5 for different values of k_r. It can be seen that the system becomes faster by increasing k_r. For $k_\mathrm{r} = 1$, the ideal system will show a deadbeat behavior and any periodic disturbance will be rejected after one period. The poles for k_r close to one (e.g., $k_\mathrm{r} = 0.9$) are located close to the stability border, which is caused by the Nth square root (19) and corresponds to slightly damped systems.

B. Dynamic Stiffness Analysis

The dynamic stiffness of the controlled system will be analyzed that expresses the disturbance rejection of the whole system [16], which is a common way to analyze the disturbance rejection ability. With the definition of the dynamic stiffness as the ratio of the disturbance to the controlled value $\mathrm{DS}(z) = \left| \frac{\underline{U}^{\mathrm{dq}}_{\mathrm{grid}}(z)}{\underline{I}^{\mathrm{dq}}_{\mathrm{grid}}(z)} \right|$, the disturbance rejection ability can be interpreted as a resistance. As a consequence, a higher distortion rejection ability at a certain frequency component has less influence on the system. For the analyzed setup, the dynamic stiffness is defined as

$$\mathrm{DS}(z) = \left| \frac{\underline{U}^{\mathrm{dq}}_{\mathrm{grid}}(z)}{\underline{I}^{\mathrm{dq}}_{\mathrm{grid}}(z)} \right| \tag{20}$$

$$\mathrm{DS}(z) = \frac{1 + \left[G_{\mathrm{RC+filter}}(z) + G_{\mathrm{PI}}(z)\right] G_{\mathrm{PWM}}(z) G_{\mathrm{Plant}}(z)}{G_{\mathrm{Plant}}(z)} \tag{21}$$

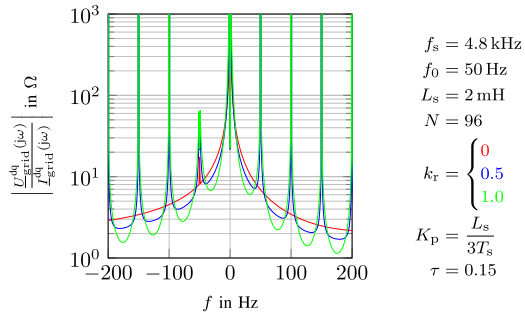

Fig. 6. Dynamic stiffness of the system with the RC.

which depends on the filter function $G_{\mathrm{RC,filter}}(z)$ and the proportional gain k_r of the RC. Hence, the filter function (15) is used. The dynamic stiffness indicates what disturbance voltage is necessary to change the grid current at a given frequency by 1 A. Thus, it is a valuable tool for analysis of voltage harmonics on current controllers. The higher the amplitude of the dynamic stiffness at a specific frequency, the better is the disturbance rejection at this frequency. It can be seen in Fig. 6 that there is high amplitude in the dynamic stiffness at the fundamental frequency f_0 for the SFPI controller, which corresponds to a high disturbance rejection ability for those frequencies. Positive frequencies correspond to positive sequences in a three-phase system and negative frequencies to negative sequences [17]. In addition, the RC provides a high stiffness at all multiples of f_0. Note, that the fundamental frequency f_0 corresponds to the dc frequency because all frequency components are shifted by 50 Hz due to the Park-transformation [18]. Furthermore, there is a significant impact on the dynamic stiffness by k_r. The higher the proportional gain k_r, the wider is the bandwidth around each resonance frequency, which leads to a better disturbance rejection for frequencies close to the resonance frequencies.

C. $T0_6$ RC Analysis

There is also a modified version of the RC described in the literature [18]–[20], which is called $\mathrm{T0}_6$ RC. If the number of delays is reduced to one sixth

$$N = \frac{f_\mathrm{s}}{6\,f_0} \tag{22}$$

the RC becomes six times faster and it has a disturbance rejection on $f = \pm 6n\,f_0,\ n \in \mathbb{Z}$ in the synchronous reference frame. This results in a disturbance rejection of the $6n \pm 1, n \in \mathbb{Z}$ harmonics in the three-phase system because of the positive and negative sequence components [18], [19]. These harmonics are exactly the occurring harmonics in a three-phase system

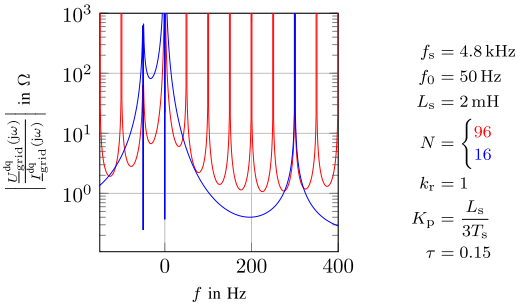

Fig. 7. Comparison of the dynamic stiffness for the standard and the $T0_6$ version of the RC.

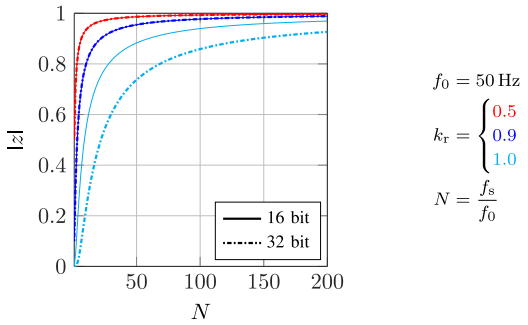

Fig. 8. Absolute value of poles for 16 bit and for 32 bit depending on N for $f_0 = 50$ Hz and on the rounding error.

TABLE I
RESOLUTION OF 16- AND 32-BIT MEMORY ACCORDING TO IEEE 754-2008

Memory width	16 bit	32 bit
Mantissa	10 bit	23 bit
Maximum rounding error	$1.95312 \cdot 10^{-3}$	$2.38419 \cdot 10^{-7}$

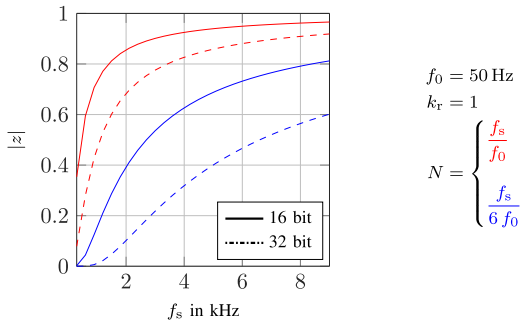

Fig. 9. Absolute value of the poles depending on the version of the RC and of the resolution with deadbeat settings, $k_r = 1$.

(5, 7, 11, 13, ...), which makes the $T0_6$ RC practical for operation at a three-phase grid.

The effect of decreasing N (22) is shown in Fig. 7 for the synchronous reference frame. The resonances at ± 300 Hz are caused by the $T0_6$ RC, whereas all frequencies in between are omitted. The band around a resonance frequency is wider for the $T0_6$ version, which results in better disturbance rejection for frequency components close to these resonance frequencies. Both the fast dynamics and the good disturbance rejection ability make the $T0_6$ RC a real alternative to the standard RC to control current harmonics. The major drawback of this particular implemented control is that even harmonics cannot be controlled any more, only the 5th, 7th, 11th, 13th, ... harmonics.

IV. Implementation Issues

Models are never perfect and therefore there will be a modeling error in each simulation. Also depending on the resolution of the used microcontroller or DSP, there are always numerical inaccuracies that result in small deviations from the original value.

A. Analysis of Numerical and Modeling Inaccuracies

As modeling errors are difficult to access in detail in the following, the focus is set on the analysis of errors due to the critical numeric precision. Typically, microcontroller systems calculate with a 16 bit or 32 bit resolution, which causes numerical errors during calculations as can be seen in Table I. Modeling errors and the limited numeric precision of the DSP or microcontroller, which run the control algorithm have a strong impact on the control design of the RC. This leads to an eigenvalue placement, which deviates from the design described in Section III of this paper.

Only numerical errors and modeling inaccuracies of the RC will be analyzed because this controller also operates at high-frequency components compared to the SPFI controller due to the zero placements along the unit circle up to high frequencies depending on N. The poles of the SFPI controller are in a much lower frequency range than the poles of the RC. AD converters can be neglected, too, due to the much higher sampling frequency of the AD converters than the frequency components of the RC. If slow AD converters are used in a setup, it has to be analyzed if the dynamic of the AD converter has to be taken into account. For that reason, smaller deviations in the controller gains, e.g., due to numerical inaccuracies, do not have a large impact here. For this reason, only the numerical error of the RC is considered in this paper. If the resolution of the AD converter is low and has an impact on the dynamics and stability, a transfer function of the AD converter can be added in the feedback path of the current control to take this into account. Then, the filter design of the RC is still straightforward with a modified open-loop transfer function $G_0(z)$.

Experimentally and by simulation, it was verified that the resolution of the DSP had a stronger impact when the AD conversion had at least 10 bit and high sampling rate.

To understand these effects, it is important to go back to the characteristic equation of the RC. If (14) and (15) are rewritten

$$z^N = 1 - k_r \frac{G_{cl}(z)}{G_{PI}(z)} \cdot G_{RC,filter}(z) \tag{23}$$

is the characteristic equation of the controlled system with

$$G_{cl}(z) = \frac{G_{PI}(z) G_{PWM}(z) G_{Plant}(z)}{1 + G_{PI}(z) G_{PWM}(z) G_{Plant}(z)}. \tag{24}$$

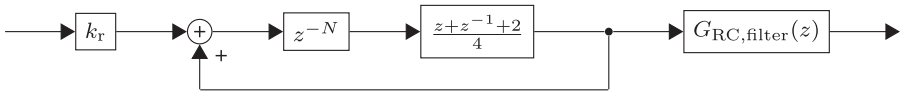

Fig. 10. RC with included low-pass filter of the first order.

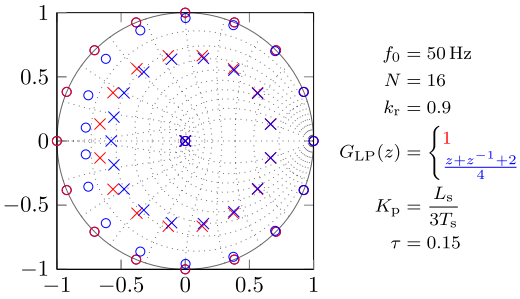

Fig. 11. Poles and zeros of the closed-loop system with and without a low-pass filter.

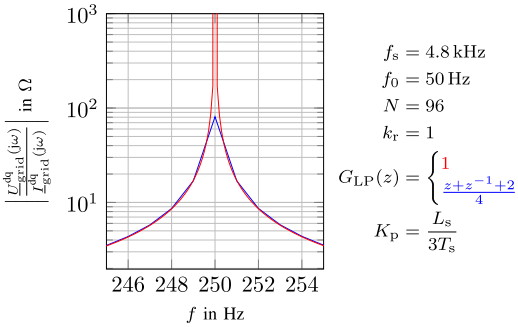

Fig. 12. Dynamic stiffness of the standard RC with and without a low-pass filter.

Considering a numerical error due to the resolution or a modeling error, (23) has to be rewritten to

$$z^N = 1 - k_\mathrm{r} \frac{G_\mathrm{cl}(z)}{G_\mathrm{PI}(z)} \left[G_{\mathrm{RC,filter}}(z) + \epsilon \cdot G_{\mathrm{RC,filter}}(z) \right] \quad (25)$$

with ϵ as the error of the filter function of the RC. Depending on the error ϵ, the poles are located at

$$z^N = 1 - k_\mathrm{r} \left(1 + \epsilon\right) \quad (26)$$

with the absolute value

$$|z| = \sqrt[N]{1 - k_\mathrm{r} \left(1 + \epsilon\right)}. \quad (27)$$

For deadbeat settings, the absolute value becomes

$$|z| = \sqrt[N]{\epsilon}. \quad (28)$$

It can be seen that there is no deadbeat behavior any more if an error exists. As can be seen in Fig. 8, small errors ϵ have a strong impact on the location of the poles especially for large values of N and therefore for high switching frequencies f_s. Due to the Nth square root, even minor deviations cause the eigenvalues to be placed quite close to the stability border.

This shows that the RC can be very effectively used for low sampling frequencies f_s, whereas with high sampling rates when

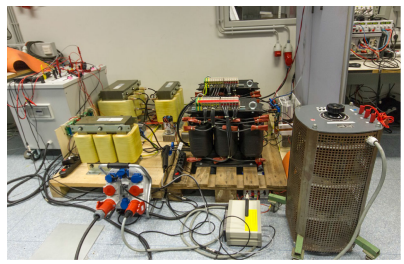

Fig. 13. Experimental setup and used parameters.

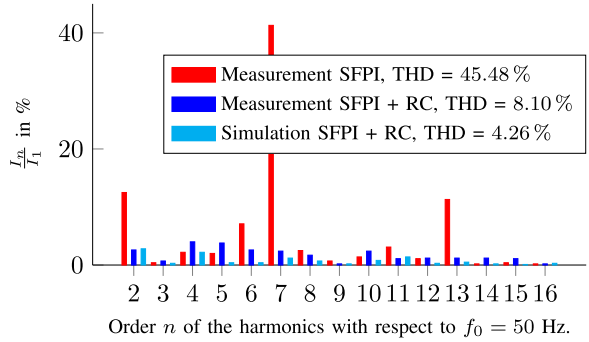

Fig. 14. Comparison of the harmonics with and without the RC in simulation and experiment corresponding to Fig. 15.

N increases, a deadbeat design is still possible, but the desired performance will be degraded due to numeric imprecision.

It can also be seen that the resolution has a significant impact for $k_\mathrm{r} = 1$. For different values of k_r, the influence of the resolution is smaller. The impact for $k_\mathrm{r} = 1$ is drawn in Fig. 9 for different resolutions.

B. RC for High Sampling Rates

If a high sampling frequency f_s is used, the poles of the closed-loop system can be found intrinsically close to the stability border due to the limited numeric precision and modeling deviations. It is possible to increase the stability of the control system with a low-pass filter placed within the RC as can be seen in Fig. 10. A typical low-pass filter used for this purpose is

$$G_\mathrm{LP}(z) = \frac{z + z^{-1} + 2}{4} \quad (29)$$

which is described in [4], [21], and [22] in detail. The phase of the frequency response function is zero for all frequencies because the transfer function is symmetric. As a result, the filter function is not causal. However, this is not a problem in the concept of the RC, because it intrinsically exhibits knowledge of the future error. The low-pass filter is placed in series to the delay elements as it is depicted in Fig. 10. The poles and zeros of the resulting system are drawn in Fig. 11

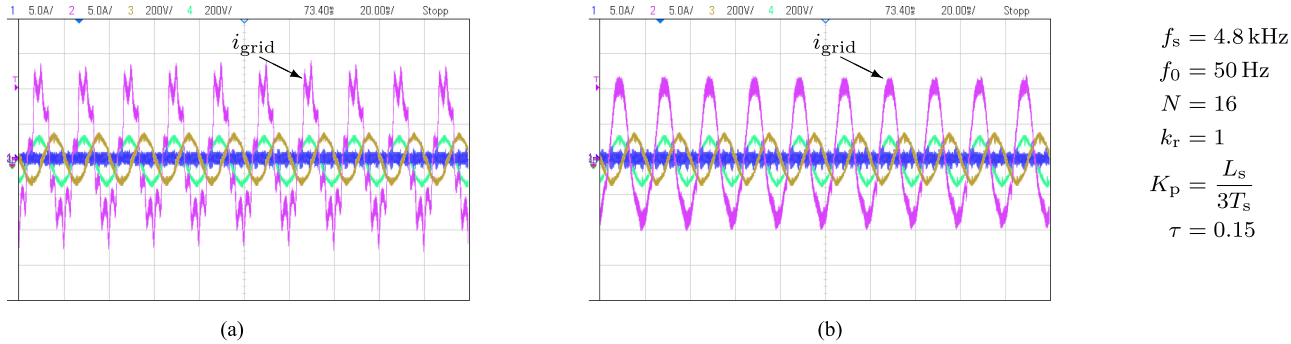

Fig. 15. Current control with (a) an SFPI and (b) with an SFPI and RC.

for $k_r = 0.9$. It can be seen that the poles and zeros from the repetitive control scheme move toward the origin, which leads to a better damping of the whole system. The damping can be further increased by using a symmetrical low-pass filter of higher order. On the other hand, the dynamic stiffness becomes worse when a low-pass filter is used as it can be seen in Fig. 12 because the amplitude at the resonance frequency is much less if the low-pass filter is used. Additionally, there is no analytic solution of the poles of the closed-loop system when a low-pass filter is used because the resulting polynomial equation cannot be solved analytically. This results in less insight of the system dynamics because the impact of the coefficients of the low-pass filter cannot be analyzed for a general system.

Similarly, modeling errors might lead to a scenario when poles are unintentionally placed slightly outside the stability border and the system becomes unstable. To prevent these system instabilities, the introduced low-pass filter is integrated in the RC in order to move the eigenvalues more into the unity circle enhancing the robustness of the system.

There are other approaches also to improve the robustness of the system with an RC with respect to model variations and numeric conditioning. If a T0_6 RC is used, the delay elements N are reduced to $1/6$ compared to the conventional RC. This leads to a significant improvement of the stability and the dynamics of the system. It can be found out that the dynamics are much less impacted by limited precision and also by small modeling errors. However, the T0_6 RC is only capable to reject multiples of the sixths harmonic in the synchronous reference frame [18].

As a third possibility to handle model deviations and numeric problems, the sampling rate itself can be reduced. If undersampling is introduced, the number of delay elements N is reduced but higher order harmonics may be omitted by the RC [23].

V. Simulations and Experiments

Simulations in MATLAB/Simulink as well as experimental results are illustrated in the following to validate the theory. Since, this paper focuses on the analysis and design of RCs, a detailed verification of the SPFI including dynamic changes has been omitted but a detailed verification of the SFPI controller with the described design method can be found in [2]. In Fig. 13, the experimental setup and the used parameters are depicted. As

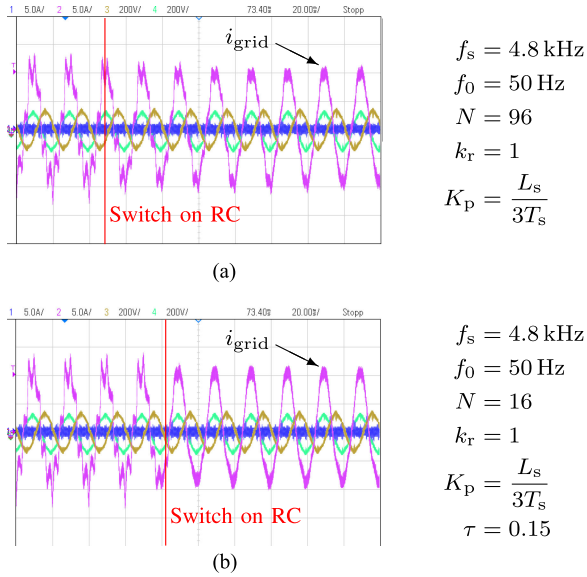

Fig. 16. Transient behavior (a) of the standard version of the RC (b) and of the T0_6 version.

a realistic setup, a diode rectifier was connected in parallel to the grid inverter to produce uneven harmonics.

In Fig. 15(a), the current is controlled to a peak value of 5 A. The current is controlled by an SFPI controller only and significant harmonics occur due to the strong excitation of the utility grid. It can be seen that in this experimental setup, the seventh harmonic is the dominant one. If the RC is used in parallel to the SFPI, it can be seen in Fig. 15(b) that the harmonics are decreased significantly. A closer look on the harmonics is given in Fig. 14. All harmonics of the grid current up to the 16th harmonic are depicted. Without the RC, strong 2nd, 7th, and 13th harmonics exist. When the RC is working, the harmonics are reduced significantly both in simulation and measurement. The current harmonics of the measurement and in the simulation agree with minor deviations demonstrating the viability of the control concept.

If the T0_6 version is used, the transient behavior and steady state can be seen in Fig. 16(b) for a peak current of 10 A. There are a lot of harmonics in the grid current before the RC is activated but after that there are much less harmonics in the current. A closer look to the steady-state current when the RC is

used shows that the current is not purely sinusoidal. Little edges can be seen beside the peaks that are caused by harmonics that are not handled by the $T0_6$ version like the fourth and ninth harmonic.

As a third example for the RC, the transient behavior of the standard version is depicted in Fig. 16(a) for a current amplitude of 10 A to explain the intrinsic delay of this controller. The RC is switched on at t_{RC}. Before t_{RC}, only the SFPI controller works and there are strong current harmonics visible. When the RC is switched ON, it takes N samples until this controller starts working because of the delay of N samples. One electric period later, the harmonics of the current are reduced significantly. The harmonics do not decay entirely because the utility grid was not stiff and the harmonics content changes over the time. Also the rounding errors result in a system that has no poles in the origin of the unit circle but close to. Nevertheless, this is quite close to the deadbeat behavior because steady state is reached after one electric period approximately.

VI. Conclusion

In this paper, it has been shown that the RC is very effective to handle and to reject current harmonics. This reduces the harmonics content in distributions grids, which leads to less THD of converters connected to those grid. The RC can be designed for the PWM converter connected to a disturbed distribution grid using a simple design approach. The dynamics of the control loop can be adjusted by one single proportional gain. A straight forward method to calculate a suitable filter function for the RC has been proposed. The impact of numerical and modeling errors has been investigated and it has been shown that the poles of the closed-loop system move to the stability border by increasing the switching frequency. A low-pass filter has been introduced to increase the stability margin of the system especially for high switching frequencies. Thereby, a combination of a low-pass filter and a $T0_6$ RC is able to increase the stability of the system significantly. However, the disturbance rejection ability becomes worse due to the low-pass filter. The introduced design approach has been validated by experiments.

References

[1] IEC, "Electromagnetic compatibility (EMC) - part 3-4: Limits - limitation of emission of harmonic currents in low-voltage power supply systems for equipment with rated current greater than 16 a."

[2] C. H. van der Broeck, R. W. De Doncker, S. A. Richter, and J. von Bloh, "Discrete time modeling, implementation and design of current controllers," in *Proc. IEEE Energy Convers. Congr. Expo.*, 2014, pp. 540–547.

[3] R. Costa-Castello, R. Grino, and E. Fossas, "Odd-harmonic digital repetitive control of a single-phase current active filter," *IEEE Trans. Power Electron.*, vol. 19, no. 4, pp. 1060–1068, Jul. 2004.

[4] M. A. Herran, J. R. Fischer, S. A. Gonzalez, M. G. Judewicz, I. Carugati, and D. O. Carrica, "Repetitive control with adaptive sampling frequency for wind power generation systems," *IEEE J. Emerg. Sel. Topics Power Electron.*, vol. 2, no. 1, pp. 58–69, Mar. 2014.

[5] P. M. de Almeida, J. L. Duarte, P. F. Ribeiro, and P. G. Barbosa, "Repetitive controller for improving grid-connected photovoltaic systems," *IET Power Electron.*, vol. 7, no. 6, pp. 1466–1474, Jun. 2014.

[6] D. Chen, J. Zhang, and Z. Qian, "An improved repetitive control scheme for grid-connected inverter with frequency-adaptive capability," *IEEE Trans. Ind. Electron.*, vol. 60, no. 2, pp. 814–823, Feb. 2013.

[7] X. H. Wu, S. K. Panda, and J. X. Xu, "Design of a plug-in repetitive control scheme for eliminating supply-side current harmonics of three-phase PWM boost rectifiers under generalized supply voltage conditions," *IEEE Trans. Power Electron.*, vol. 25, no. 7, pp. 1800–1810, Jul. 2010.

[8] M. Wu, B. Xu, W. Cao, and J. She, "Aperiodic disturbance rejection in repetitive-control systems," *IEEE Trans. Control Syst. Technol.*, vol. 22, no. 3, pp. 1044–1051, May 2014.

[9] M. Li, W. Li, C. Liu, J. Wei, and T. Chen, "Comparison of two repetitive control strategies of ups inverter on saber," in *Proc. 6th Int. Forum Strategic Technol.*, Aug. 2011, vol. 1, pp. 575–579.

[10] C.-Y. Lin and H.-Y. Yeh, "Repetitive model predictive control based on a recurrent neural network," in *Proc. Int. Symp. Comput., Consum. Control*, Jun. 2012, pp. 540–543.

[11] M. Morimoto, T. Zanma, M. Ishida, G. Pipeleers, and J. Swevers, "Suppression of harmonic current for IPMSM using generalized repetitive control," in *Proc. IEEE Int. Conf. Ind. Technol.*, 2002, pp. 264–267.

[12] P. Mattavelli and F. P. Marafao, "Repetitive-based control for selective harmonic compensation in active power filters," *IEEE Trans. Ind. Electron.*, vol. 51, no. 5, pp. 1018–1024, Oct. 2004.

[13] P. Schuelting, C. H. van der Broeck, and R. W. De Doncker, "A generalized control design approach for a repetitive controller on current harmonics," in *Proc. IEEE 16th Workshop Control Model. Power Electron.*, Jul. 2015, pp. 1–8.

[14] Q. Liu, Y. Wang, W. Liu, and H. Ma, "A fixed-frequency quasi sliding-mode repetitive control (QSMRC) for voltage source inverters," in *Proc. 1st Int. Future Energy Electron. Conf.*, Nov. 2013, pp. 711–715.

[15] R. Merry, D. Kessels, R. van de Molengraft, and M. Steinbuch, "Repetitive control applied to a walking piezo actuator," in *Proc. IEEE Int. Conf. Control Autom.*, Dec. 2009, pp. 854–859.

[16] J. S. Lee and R. D. Lorenz, "Robustness analysis of deadbeat-direct torque and flux control for IPMSM drives," *IEEE Trans. Ind. Electron.*, vol. 63, no. 5, pp. 2775–2784, May 2016.

[17] C. H. van der Broeck, M. Biskoping, and R. W. D. Doncker, "Discrete time control design of three phase PWM rectifiers," in *Proc. 17th Eur. Conf. Power Electron. Appl.*, Sep. 2015, pp. 1–10.

[18] D. Chen, J. Zhang, and Z. Qian, "Research on fast transient and $6n \pm 1$ harmonics compensating repetitive control scheme for three-phase systems," in *Proc. IEEE Energy Convers. Congr. Expo.*, Sep. 2012, pp. 4746–4753.

[19] S. Jiang, D. Cao, Y. Li, J. Liu, and F. Z. Peng, "Low-THD, fast-transient, and cost-effective synchronous-frame repetitive controller for three-phase UPS inverters," *IEEE Trans. Power Electron.*, vol. 27, no. 6, pp. 2994–3005, Jun. 2012.

[20] G. Escobar, M. Hernandez-Gomez, A. Valdez-Fernandez, M. Lopez-Sanchez, and G. Catzin-Contreras, "Implementation of a $6n \pm 1$ repetitive controller subject to fractional delays," *IEEE Trans. Ind. Electron.*, vol. 62, no. 1, pp. 444–452, Jan. 2015.

[21] C. Cosner, G. Anwar, and M. Tomizuka, "Plug in repetitive control for industrial robotic manipulators," in *Proc. IEEE Int. Conf. Robot. Autom.*, May 1990, vol. 3, pp. 1970–1975.

[22] Y. Wang, D. Wang, and X. Wang, "A three-step design method for performance improvement of robust repetitive control," in *Proc. Am. Control Conf.*, Jun. 2005, vol. 2, pp. 1220–1225.

[23] Z. Cao and G. Ledwich, "Adaptive repetitive control to track variable periodic signals with fixed sampling rate," *IEEE/ASME Trans. Mechatronics*, vol. 7, no. 3, pp. 378–384, Sep. 2002.

Philipp Schülting received the B.Sc. and M.Sc. degrees in electrical engineering from RWTH Aachen University, Aachen, Germany, in 2014.

Since January 2015, he has been with the Institute for Power Electronics and Electrical Drives, RWTH Aachen University. His research interests include the field of power electronics and control.

Christoph H. van der Broeck received the B.Sc. and M.Sc. degrees in electrical engineering from RWTH Aachen University, Aachen, Germany, in 2010 and 2013. Since January 2014, he has been working toward the Ph.D. degree with the Institute for Power Electronics and Electrical Drives, RWTH Aachen University.

From 2011 to 2012, he was with the Wisconsin Electric Machine and Power Electronic Consortium, University of Wisconsin, Madison, as a Fulbright Scholar. Between 2012 and 2013, he was with AixControl GmbH on control design of power converters. His research interests include the modeling and control of power electronic converters and drives.

Rik W. De Doncker received the Ph.D. degree in electrical engineering from the Katholieke Universiteit Leuven, Leuven, Belgium, in 1986.

In 1987, he was appointed as a Visiting Associate Professor with the University of Wisconsin, Madison. After a short stay as an Adjunct Researcher with IMEC, Leuven, Belgium, he joined the Corporate Research and Development Center, General Electric Company, Schenectady, NY, USA, in 1989. In 1994, he joined Silicon Power Corporation, a former division of General Electric Inc., as the Vice President of Technology. He is currently a Professor with RWTH Aachen University, Aachen, Germany, where he leads the Institute for Power Electronics and Electrical Drives. In 2006, he also became the Director of the E.ON Energy Research Center, RWTH Aachen University.

Dr. Doncker was the President of the IEEE Power Electronics Society (PELS) in 2005 and 2006. He was the founding Chairman of the German IEEE Industry Applications Society (IAS) PELS Joint Chapter. In 2002, he received the IAS Outstanding Achievement Award. In 2008, he received the IEEE Power and Energy Society Nari Hongorani Custom Power Award. In 2009, he led a VDE/ETG Task Force on Electric Vehicles. In 2010, he received the Honorary Doctor degree from Technical University Riga, Riga, Latvia. In 2010, he became member of the German National Platform for Electromobility.